LA-UR-85-1460 CONF-8411153--4 RECEIVED BY OSTI MAY 0 6 1985

Los Alamos National Laboratory is operated by the University of California for the United States Department of Energy under contract W-7405-ENG-36.

LA-UR--85-1460

DE85 010736

TITLE: RECENT RESULTS OF THE LOS ALAMOS FREE-ELECTRON LASER OSCILLATOR EXPERIMENT

AUTHOR(S): R. L. Sheffield, AT-7, R. W. Warren, AT-7, B. E. Newnam, CHM-6, W. E. Stein, AT-7, J. C. Goldstein, X-1, M. T. Lynch, AT-5

SUBMITTED TO: International Conference on Lasers '84
Society for Optical and Quantum Electronics
San Francisco, CA, November 26-30, 1984.

DISCLAIMER

Los Alamos Los Alamos National Laboratory
Los Alamos, New Mexico 87545

FORM NO 836 R4
ST NO 2629 5/81

RECENT RESULTS OF THE LOS ALAMOS FREE-ELECTRON LASER OSCILLATOR EXPERIMENT*

R. L. Sheffield, R. W. Warren, B. E. Newnam, W. E. Stein,
J. C. Goldstein, and M. T. Lynch, AT-7, MS H825
Los Alamos National Laboratory, Los Alamos, NM 87545

Abstract

Since the last Lasers '83 Conference, significant progress has been made on the Los Alamos free-electron laser (FEL). Although the previously reported results were in agreement with theory, the data were plagued by gain fluctuations, and no spectral measurements had been obtained. Since then, the source of the fluctuations has been analyzed and substantially reduced. Also, the optical power and spectra dependence on beam emittance, alignment, cavity length, energy spread, and current were systematically studied. This paper reports on the results obtained with a uniform-period wiggler.

Introduction

This paper is divided into two sections: The first section covers electron-beam performance and electron-beam energy-distribution measurements, with and without laser oscillation; the second section discusses optical results. The electron-beam energy measurements showed that 1% of the power was extracted from a 1-MW (average over a 100-μs macropulse) electron beam.

The optical results included the following:

- Small-signal gain up to 60%
- Wavelength tuning range of 9 to 35 μm
- Strong Raman sidebands in the optical spectra
- Cavity-length detuning curves in general agreement with theory
- Strehl ratio of 0.9
- Optical peak power of 10 MW
- Observation of the second and third harmonics

Experimental Apparatus

The apparatus was described in detail at last year's conference;[1] therefore, only a brief description will be given in this paper. This experiment[2] used a conventional rf accelerator, a 1-m uniform-period wiggler, and operated at a nominal 10-μm wavelength. The major characteristics and parameters of the FEL oscillator system are listed in Table I. A plan view of the major components of the accelerator, the wiggler, and the optical cavity is shown in Fig. 1. A more detailed view of the beamline section containing the major electron diagnostics is shown in Fig. 2. Temporal characteristics (Fig. 3) of the electron beam's 100-μs macropulse are 2000 36-ps micropulses separated by 46 ns.

Electron Beam Measurements

The electron-beam diagnostics[3] consisted of standard beam-current, spatial-position, and spatial-profile monitors and a time-resolvable beam-energy spectrometer. This section will discuss the results obtained with the beam-profile monitors and the spectrometer.

The profile monitors were Suprasil quartz plates combined with a vidicon camera viewing the Cerenkov light produced by the passage of the electron beam through the quartz. Two of these monitors were used in conjunction with an upstream quadrupole lens to determine the electron-beam emittance. By varying the quadrupole field strength, a waist was formed at one of the monitors. The unnormalized emittance ϵ was then calculated from the expression $\epsilon = \pi D_1 D_2/4S$, where D_1 and D_2 are the beam diameters at the two monitors and S is the separation of the monitors. The beam emittance as a function of the gun current is shown in Fig. 4. The extraction-efficiency measurements were taken at an emittance of 2.5 π•mm•mrad (40-A micropulse current).

The time-resolvable beam-energy diagnostics provided a three-dimensional presentation of the electron current as a function of energy and time. A quartz screen was located at the focal plane of the energy spectrometer. The Cerenkov light produced by the electron beam

*This work was performed under the auspices of the US Dept. of Energy and supported by the US Army Ballistic Missile Defense Organization.

TABLE I

EXPERIMENTAL PARAMETERS

Optical	
Wavelength	9-11 μm, dielectric mirrors and 9-35 μm, copper mirrors
Cavity length, L_C	6.92 m
Mirror reflectance (at 10.5 μm)	99.8%, rear; choice of 95%, 97.5% or 99.8% front coupler
Mirror reflection bandwidth	20%
Rayleigh range, z_F	0.63 m
Undulator	
Magnets	$SmCo_5$, 0.5 X 0.5 X 3.5 cm
Length	100 cm
Period	2.73 cm, constant
Number of periods	37
Gap between magnets	8.8 mm
Peak magnetic field	0.3 T
Undulator parameter, a_w	0.76
Electron Beam	
Electron energy	21.0 MeV at 10.5 μm, 11.5- to 23-MeV tuning range
Accelerator frequency	1.3 GHz
Micropulse spacing	46.2 ns
Micropulse width (FWHM)	36 ± 5 ps (Lorentzian shape)
Charge/micropulse	2.4 nC std.; up to 3.2 nC
Peak current	40 A std; up to 50 A
Macropulse length	100-120 μs (>2000 micropulses)
Repetition rate	1 Hz
Energy spread	2% FWHM standard; 1-3% variable range
Emittance	2.5-5.5 π•mm•mrad

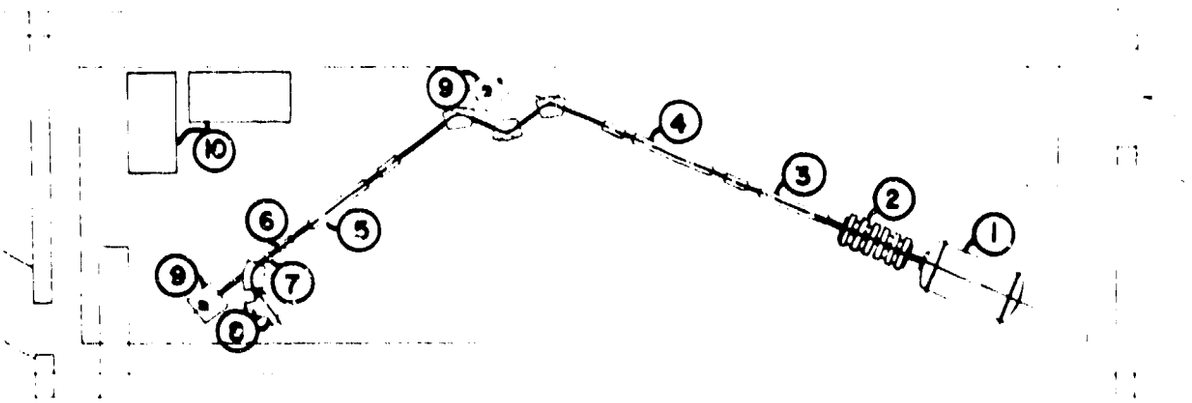

Fig. 1. Experimental arrangement of the Los Alamos FEL. Numbers designate (1) 80-keV electron gun, (2) 108- and 1300-MHz bunchers, (3) 10-MeV linac tank, (4) 11-MeV linac tank, (5) undulator, (6) slow vertical deflector (7) 1300-MHz vertical deflector, (8) electron spectrometer, (9) optical resonator mirrors, and (10) optical diagnostics and resonator alignment tables.

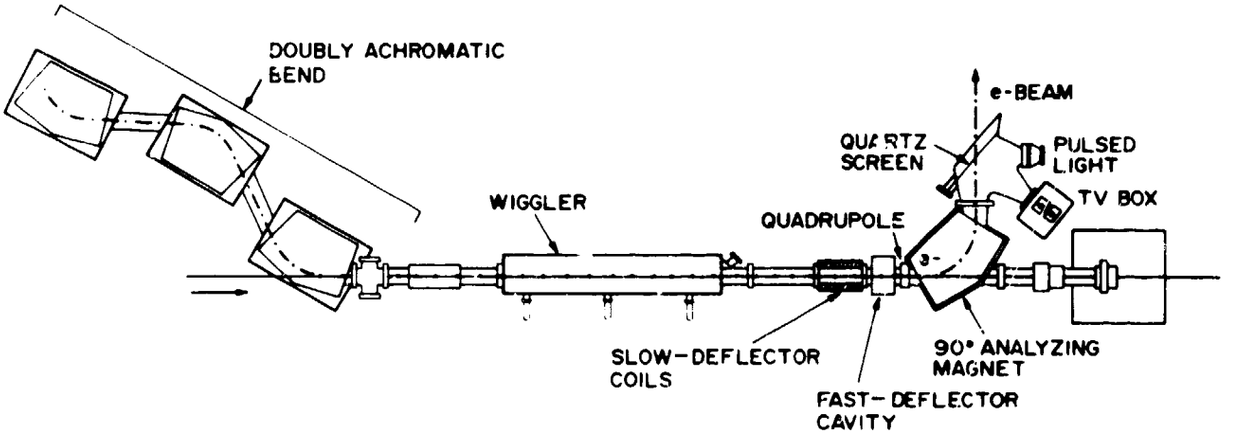

Fig. 2. Part of beamline including 60° bends, wiggler, slow and fast deflector, quadrupole magnet, and spectrometer system.

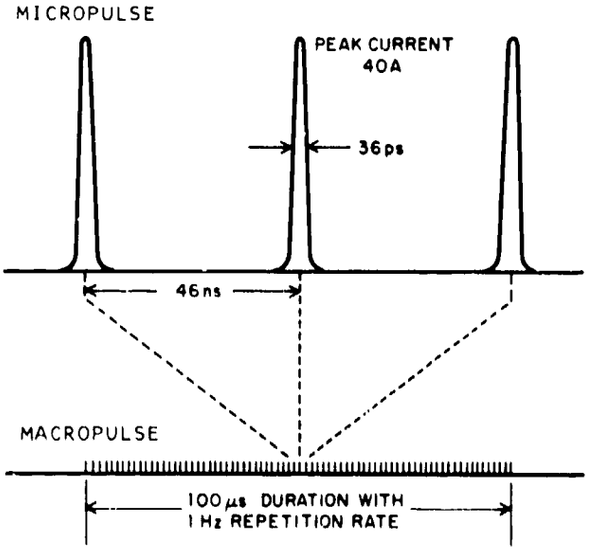

Fig. 3. Schematic diagram illustrating the 1-s, 100-μs, 46-ns, and 36-ps time intervals.

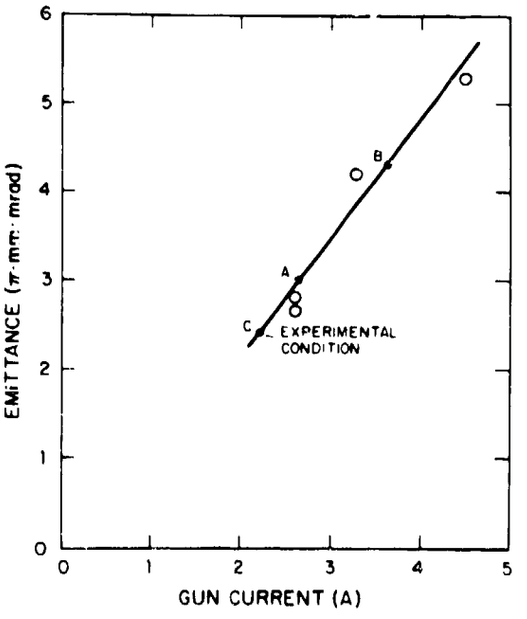

Fig. 4. Emittance measured after the accelerators as a function of gun current. A is the normal operating point; B is used when high laser gain and output power are desired; C is used when good emittance and high-energy extraction are desired.

passing through the quartz screen was viewed by two gateable, microchannel-plate intensifiers optically coupled to vidicon TV cameras. The energy distribution was obtained by a horizontal dispersion of the electrons in a 90° magnetic spectrometer, and the time resolution was produced by a vertical deflection of the beam. Two separate, vertical-deflection devices covered different time domains. A pulsed electromagnetic dipole (slow deflector) covered between 10 and 100 μs, and an rf cavity (fast deflector) covered between 10 and 100 ps.

The beamline downstream from the accelerators is shown in Fig. 2. First in line are the three 60° nonisochronous, doubly achromatic, bending magnets. The magnets bring the electron beam into the optical resonator and, in conjunction with a slit system, remove undesirable low-energy electrons from the beam. Next in the beamline is the wiggler followed by the slow deflector, fast deflector, diagnostic quadrupole, and the 90° spectrometer magnet with its focal-plane quartz screen.

The diagnostic quadrupole served two purposes: First, it permitted adjustment of the axial position of the electron-beam waist and, as a consequence, optimized either the vertical (time) resolution or horizontal (energy) resolution. Second, the quadrupole increased the vertical deflection of the beam at the target screen and provided better vertical (time) resolution.

One of the two vidicons viewing the focal-plane screen had a wide field of view and was used with the slow deflector. The other camera had a smaller field of view (greater magnification) and, when used with the fast deflector, was operated in the gated mode. The overall resolution of the camera systems was limited by the electron-beam spot size.

A diagram showing how the slow deflector produced a deflection of the beam at the focal-plane screen is shown in Fig. 5. The construction of the slow deflector is discussed in Ref. 3. The TV image from the slow-deflector monitor cannot be reproduced for publication with acceptable quality. Therefore, Fig. 6 is shown as an artist's reproduction of the pattern produced on the TV monitor. By taking a cross section through the three-dimensional representation along the energy axis, the electron distribution can be obtained at the time indicated by T_C on the time axis on Fig. 6a. Without laser oscillation, the electron distribution had a 2% FWHM energy spread. When oscillation occurred, the electron energy distribution was shifted downward and was distorted in accordance with the transfer of energy to the photon beam (Fig. 6b).

For beam conditions optimal for strong laser oscillation (peak micropulse current of 40 A), the energy spectra at the time corresponding to peak laser intensity were plotted with and without oscillation as in Fig. 7. The data for several sequential macropulses were superimposed for this measurement; the low-energy tail of the electron distribution was removed by a scraper in the 60° achromatic bends. The energy change caused by the laser oscillation, as well as the reproducibility of the data, is evident. The measured extraction efficiency of 1.0 ± 0.2% was determined from the shift in the average energy of these two curves.

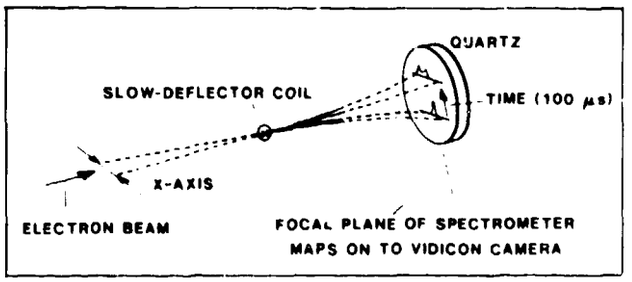

Fig. 5. Schematic view of slow deflector and quartz screen.

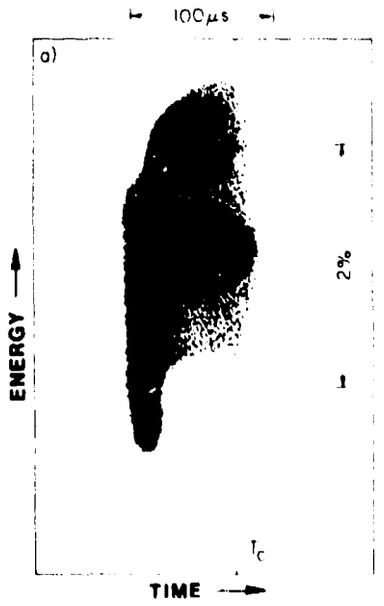

Fig. 6a. Display of current density versus energy and time during a macropulse without laser oscillation; T_C indicates the time at which the energy distribution was obtained.

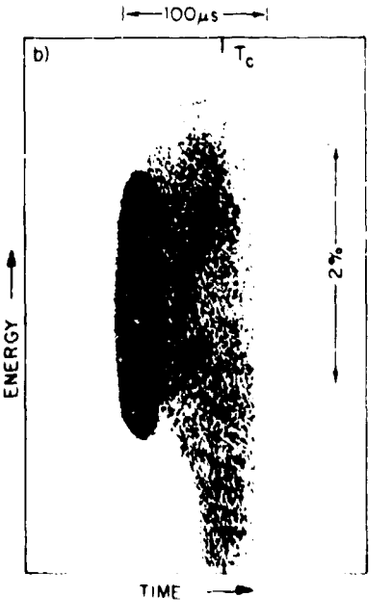

Fig. 6b. Display of current density versus energy and time during a macropulse with laser oscillation; T_C indicates the time at which the energy distribution was obtained.

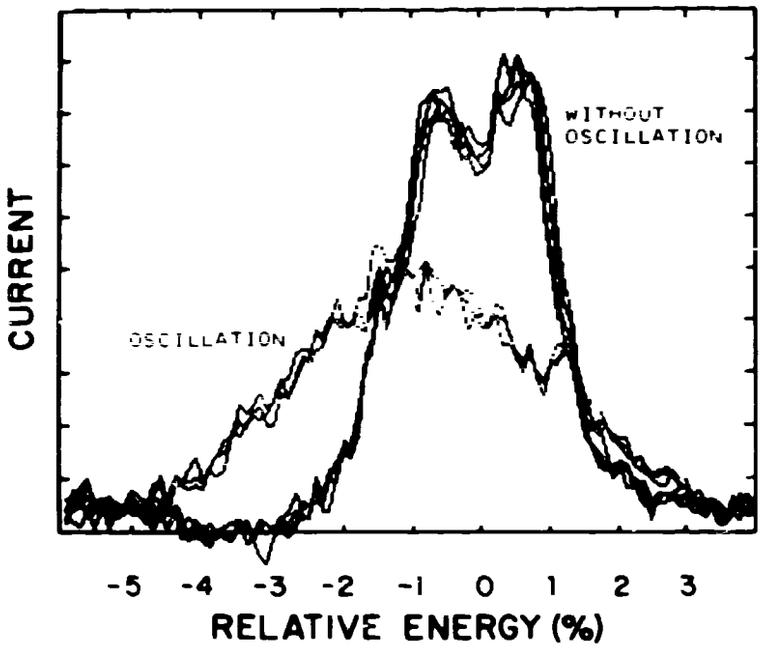

Fig. 7. Energy distributions with and without laser oscillation averaged over many micropulses. Six spectra of each kind are superimposed.

The fast deflector gave the electron current as a function of time and energy during individual micropulses. The electron beam was vertically deflected in the magnetic field of an rf resonant cavity driven at the fundamental frequency of the accelerators. Operating in a manner analogous to the slow deflector, the fast deflector gave a 3-D representation on the quartz screen of the electron current as a function of both energy and time except in the picosecond range. The microchannel-plate-intensified vidicon was gated to view either a single or group of micropulses at any time during the 100-μs macropulse. The construction details for the fast deflector are given in Ref. 3.

An artist's reproduction of the three-dimensional micropulse presentation on the fast-deflector monitor is shown in Fig. 8a. The current density is indicated by the shading. The dashed line traces the crest of the current distribution. The curve follows the variations of the accelerator field and approximates a cosine function. It is, however, double valued in time. The rotation of the cosine function is a consequence of the nonisochronism of the 60° achromatic bends. Higher energy electrons bend less and so take less time to traverse the bends. Thus, the energy-time curve differs before and after the 60° bends. This difference is manifested by a horizontal shift of the time axis to later times by 26 ps for every 1% of energy drop.

Laser oscillation will occur only when the electron current is sufficient to provide adequate gain. Therefore, energy extraction in the micropulse will only occur for those electrons that have a current above a threshold value determined by the optical cavity losses. This condition is evident in Fig. 8b where oscillation coincided with the peak of the electron density, only those electrons at the peak were dispersed toward lower energies. The dispersed low-energy tail was not rotated toward later time as were the early and late tails in the primary distribution because the energy extraction occurred in the wiggler, which was downstream from the nonisochronous 60° bends.

A cross section was made at time T_c (the peak of the electron density) with and without oscillation. In this measurement the FEL was oscillating weakly, and low-energy electrons were not removed by the scraper. A 0.4% energy-extraction efficiency was measured for this small interval (~20 ps) within the micropulse. The extraction efficiency for the whole micropulse was 0.2%.

The temporal pulse shape (that is, current versus time) of a micropulse was measured using the fast deflector. An integration of the distribution over energy results in a distribution of electron current as a function of time. The correct temporal profile was obtained by measuring the pulse shape with the fast deflector off and deconvolving the pulse duration (shown in Fig. 9) of 36 ps (FWHM). Performing the same operation on the dispersed tail present during oscillation showed that only the electrons in the central 20 ps (or less) of the pulse contributes to oscillation. An improvement in the time resolution will be required to accurately measure the duration of oscillation in future experiments.

Optical Measurements

The optical measurements are addressed in the following order: small-signal gain, energy and power output, cavity-length detuning, Raman sidebands, optical harmonics, wavelength tuning, and spatial beam quality.

The small-signal gain depends strongly on the peak electron current, and maximum values of 15 and 60% were measured for respective peak currents of 30 and 50 A. Representative data of the growth from incoherent spontaneous emission to exponential gain are shown in Fig. 10. For this case, a small-signal gain of 45% was measured by a Hg:Ge photodetector (after correcting for detector nonlinearities).

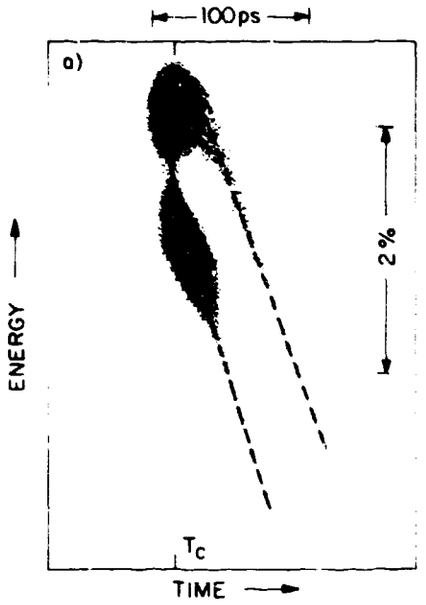

Fig. 8a. Display of current density versus energy and time in a micropulse without laser oscillation; T_c indicates the time at which the energy distribution was obtained.

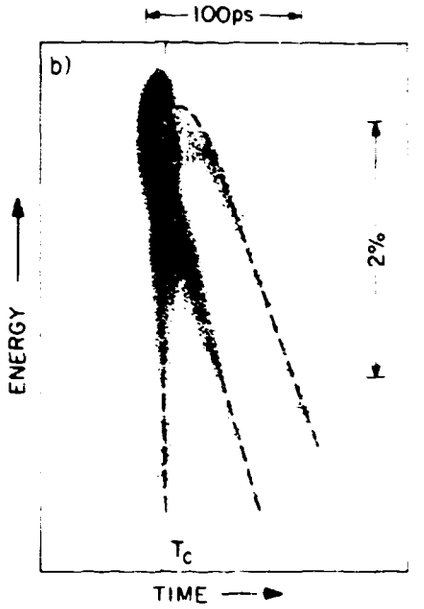

Fig. 8b. Displa, of current density versus energy and time in a micropulse with laser oscillation; T_c indicates the time at which the energy distribution was obtained.

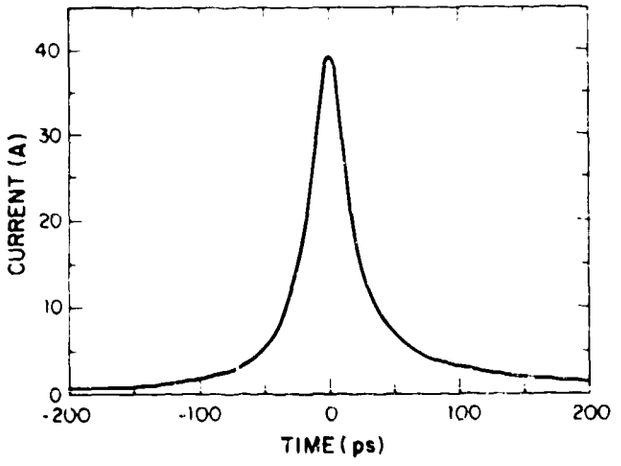

Fig. 9. Current distribution in a micropulse versus time.

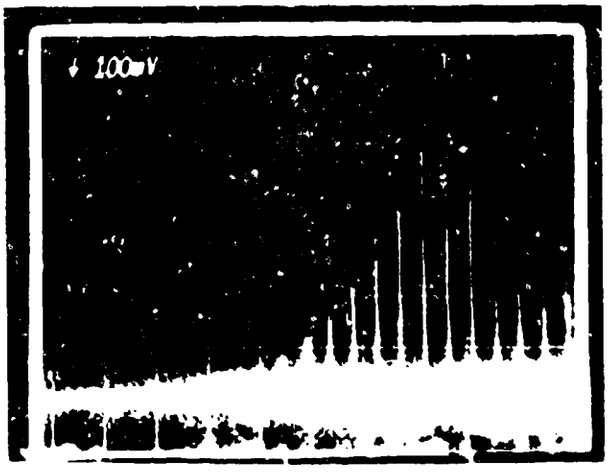

Fig. 10. Exponential rise of the optical micropulse energy from spontaneous emission en route to saturation. A net small-signal energy gain of 34% per cavity round trip is represented.

The results of the energy and power measurements are summarized in Table II. The total optical energy integrated over a macropulse was measured using a Scientech calorimeter, supplemented by a Gentec pyroelectric energy meter. Using the initial electron-beam power (calculated from the measured beam current and energy) the optical measurements gave, for a 7% output coupler, an energy-extraction efficiency of 0.6%; however, no corresponding measurements of energy extraction from the electron beam were made for this case. For a nominal 0.25% coupler, the optical measurements gave an energy-extraction efficiency of 1.1 ± 0.1%. This result is to be compared with the energy-extraction efficiency of 1.0 ± 0.2% measured directly by the electron spectrometer.

TABLE II

BEST OSCILLATION RESULTS FOR 30- AND 40-A PEAK CURRENTS

Output coupler transmittance (%)[a]	0.25	7
Power decay rate from optical cavity (%)	≥1.6	7.5
Micropulse peak current (s)	27	~40
Net small-signal energy gain (%)[b]	5	≤40
Duration of lasing macropulse (μs)	70	90
Average output power (kW)[c]	1.3	6
Peak output power (MW)[c,d]	2	10
Peak intracavity power (MW)[c,d]	800	140
Extraction efficiency (%)		
From laser energy output:[c]	1.1 ± 0.1	0.6
Computed from electron-beam energy spectrum:[e]	1.0 ± 0.2	not measured
Cavity tuning range (μm)	80-100	55-60

[a]Average over the width of the spectral output.

[b]Less than theoretical predictions because of the fast-rising electron energy at the start of the macropulse.

[c]Average over the entire optical macropulse.

[d]A 30-ps optical pulse assumed for this calculation. Peak powers twice the values given were predicted for the 1- to 2-ps substructure associated with the observed spectra.

[e]Maximum value during the macropulse.

A typical cavity-length detuning curve is shown in Fig. 11. The saturated optical power is plotted against cavity length. The zero of the length (horizontal) scale corresponds to the maximum laser power. The electron energy was selected to obtain essentially constant cavity-mirror reflectance over the entire bandwidth of generated wavelengths.

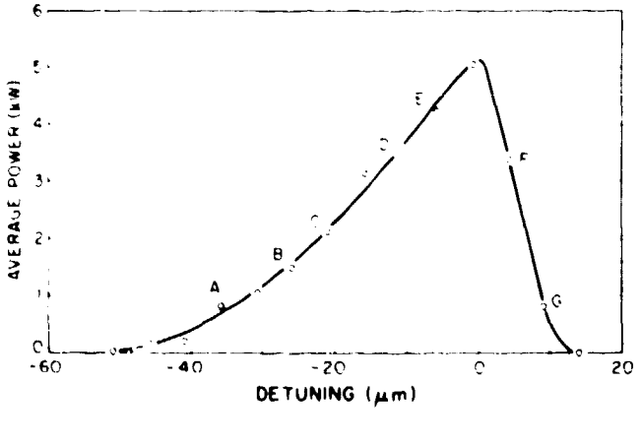

Fig. 11. Resonator cavity-length detuning dependence. Negative lengths indicate short cavity.

Two Raman spectra are presented in Fig. 12. Each spectrum is integrated over an entire macropulse. A minimum spectral width of 0.3% FWHM (Fig. 12a) was obtained when the laser was forced to oscillate near threshold, either by cavity detuning or reduced electron current. However, for normal operation (high optical power) the spectral FWHM (Fig. 12b) was 2-4%. Significant variations in both the width and structure occurred shot-to-shot, caused in part by electron-bunch phase and amplitude jitter of the electron beam.

Coherent spontaneous emission at harmonic wavelengths of the fundamental oscillation wavelength was due to deviations from sinusoidal motion of bunched electrons within the undulator. The coherent spontaneous emission was detected using a high-rejection filter in front of a sensitive Hg:Ge detector (to block the fundamental 10.5-μm radiation). The detected signal exhibited the following properties: In contrast to the gradual exponential decay at the end of a macropulse characteristic of the fundamental, (Fig. 13), the filtered optical power exhibited a sudden

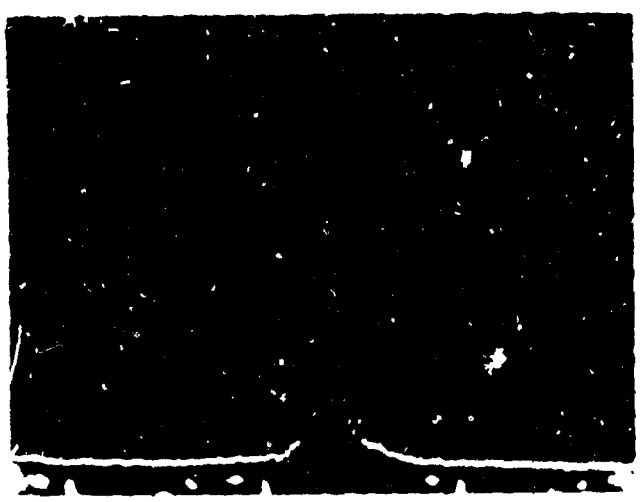

Fig. 12a. Single-peak spectrum observed at 10.6 μm for lower power oscillation attained by detuning (shortening) the cavity length. A FWHM of 0.5% was observed here; 0.3% was the minimum observed during these experiments.

Fig. 12b. Multipeak spectrum of the high-power laser output, characteristic of the Raman instability, attained with an optimum cavity length (zero detuning). This oscillogram displays a FWHM of 4% for the entire spectrum centered at 10.5 μm.

Fig. 13. Exponential decay of the laser output power after the end of the electron-beam macropulse. The 1.2-μs decay time corresponds to 3.5% loss per resonator-cavity round trip when the output coupler transmission was ~2.5%.

drop after the last current micropulse followed by an exponential decay faster than that of the fundamental; this behavior was due to the dielectric mirror reflectance at the second and third harmonics (high reflectance at the third harmonic and very low reflectance at the second harmonic). For both harmonics, the macropulse envelope was modulated with high-frequency noise (Fig. 14) not observed on the fundamental macropulse envelope. Using moderately narrow-band interference filters and a Hg:Ge detector, the total power level of the second and third harmonics exiting both resonator mirrors was measured to be ~10^{-5} that of the fundamental.

For the wavelength tuning experiment, the optical resonator was configured with uncoated copper mirrors to enable the resonator to oscillate over a large spectral bandwidth. The light was coupled out through an axial hole that transmitted 2.4% at 10.6 μm. By varying the electron energy, the wavelength of the laser radiation was tuned continuously from 9 to 35 μm, a factor of 4. Direct detection of the laser radiation over this bandwidth was not possible because the Hg:Ge detector and the ZnSe output window have wavelength cutoffs at 16 and 22 μm, respectively. Instead, the presence of longer wavelength oscillation was inferred by the following: first, the electron beam was tuned to energies corresponding to longer wavelengths; second, measurement of the electron energy spectrum showed substantial energy extraction over the entire tuning range; third, the detected macropulse envelope had the power and high-frequency noise consistent with harmonics of the fundamental; fourth, as the wavelength increased, the total cavity loss decreased (reduced transmission through

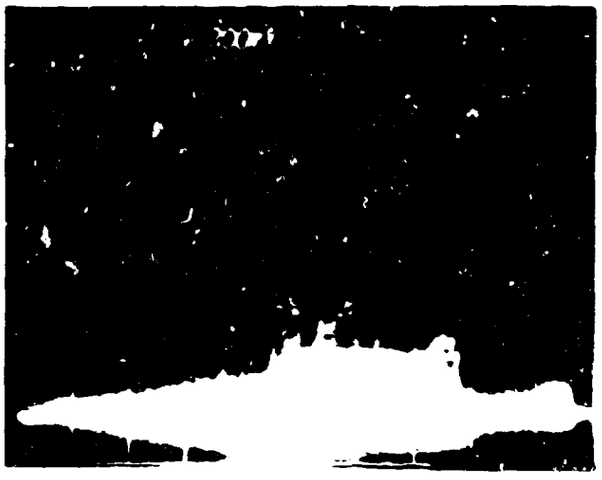

Fig. 14. Laser power versus time of coherent spontaneous emission at the second harmonic wavelength at 5.2 μm. The oscillogram shows high-frequency noise on the envelope of the pulse train, a characteristic of all harmonic emission observed.

the output coupler at longer wavelengths). Almost no realignment and refocusing of the electron beam were required to change the electron-beam energy by the factor of 2 necessary to tune the oscillator from 9 to 35 μm. With more experience in properly bunching and transporting a lower energy electron beam through the 60° bending magnets, we believe that the tuning range of this system could be extended to wavelengths approaching 100 μm.

The Strehl ratio (ratio of the focal-plane axial intensity of the measured beam to an unaberrated Gaussian beam with the same divergence at the lens plane) of the optical beam was measured to be 0.9. The result was independent of the magnitude of the Raman sideband instability. This ratio corresponds to a net phase distortion of $\lambda/20$ and could have been due to imperfections in the cavity mirrors or external optics. The transmitted beam energy through a 1.6-mm-diam aperture in the focal plane was 99%. This transmittance is very close to the 99.7% theoretical transmittance calculated for a Gaussian beam with the same spot size.

Summary

The recent results of the Los Alamos FEL oscillator experiment have been summarized. The problems discussed at last year's conference have been resolved, and significant progress has been made in understanding operation of our FEL. The most interesting results include small-signal gains up to 60%, electron-energy extraction efficiency of 1.0 ± 0.2%, 10-MW peak output power, 6-kW average power for a 90-μs macropulse, Strehl ratio of 0.9, observation of the second and third harmonics, observation of the Raman sideband instability, and tuning of the oscillator wavelength from 9 to 35 μm by varying the electron-beam energy from 23 to 12 MeV.

Acknowledgments

We wish to thank those who helped in the design, construction, and operation of this experiment, in particular, J. S. Fraser, J. G. Winston, A. H. Lumpkin, P. J. Tallerico, A. C. Saxman, P. M. Giles, and L. M. Young. We are also grateful for the technical contributions and cooperation of O. R. Norris, J. R. Chavez, T. O. Gibson, J. O. Hornkohl, C. M. Humphry, and M. C. Whitehead. Assistance in data reduction was given by D. W. Feldman and S. A. Apgar. The leadership and encouragement of J. M. Watson and C. A. Brau was important for the successful completion of this experiment and is greatly appreciated.

References

1. R. W. Warren, B. E. Newnam, W. E. Stein, J. G. Winston, R. L. Sheffield, M. T. Lynch, J. C. Goldstein, M. C. Whitehead, O. R. Norris, G. Luedemann, T. O. Gibson, and C. M. Humphry. "First Operation of the Los Alamos Free-Electron Laser Oscillator," Proc. of the Int. Conf. on LASERS '83, 316 (1984).

2. R. W. Warren, J. S. Fraser, W. E. Stein, J. G. Winston, T. A. Swann, A. H. Lumpkin, R. L. Sheffield, J. E. Sollid, B. E. Newnam, C. A. Brau, and J. M. Watson, "The Los Alamos Free-Electron Laser Oscillator Experiment: Plans and Present Status," SPIE Vol. 453, 130 (1984).

3. R. L. Sheffield, W. E. Stein, A. H. Lumpkin, R. W. Warren, and J. S. Fraser, "Electron Beam Diagnostics for the Los Alamos Free-Electron Laser Oscillator Experiment," SPIE Vol. 453, 151 (1984).